JACS
JOURNAL OF THE AMERICAN CHEMICAL SOCIETY
Article
pubs.acs.org/JACS

Two BN Isosteres of Anthracene: Synthesis and Characterization

Jacob S. A. Ishibashi,[†,‡,⊥] Jonathan L. Marshall,[†,⊥] Audrey Mazière,[§] Gabriel J. Lovinger,[†,‡] Bo Li,[‡] Lev N. Zakharov,[†] Alain Dargelos,[§] Alain Graciaa,[§] Anna Chrostowska,*[,§] and Shih-Yuan Liu*[,†,‡]

[‡]Department of Chemistry, Merkert Chemistry Center, Boston College, Chestnut Hill, Massachusetts 02467-3860, United States
[†]Department of Chemistry and Biochemistry, University of Oregon, Eugene, Oregon 97403, United States
[§]Institut des Sciences Analytiques et de Physico-Chimie pour l'Environnement et les Matériaux, UMR CNRS 5254, Université de Pau et des Pays de l'Adour, Avenue de l'Universite, 64 000 Pau, France

Supporting Information

ABSTRACT: The synthesis of two parental BN anthracenes, **1** and **2**, was developed, and their electronic structure and reactivity behavior were characterized in direct comparison with all-carbon anthracene. Gas-phase UV-photoelecton spectroscopy studies revealed the following HOMO energy trend: anthracene, −7.4 eV; BN anthracene **1**, −7.7 eV; bis-BN anthracene **2**, −8.0 eV. The λ_{max} of the lower energy band in the UV−vis absorption spectrum is as follows: anthracene, 356 nm; BN anthracene **1**, 359 nm; bis-BN anthracene **2**, 357 nm. Thus, although the HOMO is stabilized with increasing BN incorporation, the HOMO−LUMO band gap remains unchanged across the anthracene series. The emission λ_{max} values for the three investigated anthracene compounds are at 403 nm. The pK_a values of the *N*-H proton for BN anthracene **1** and bis-BN anthracene **2** were determined to be approximately 26. BN anthracenes **1** and **2** do not undergo heat- or light-induced cycloaddition reactions or Friedel−Crafts acylations. Electrophilic bromination of BN anthracene **1** with Br_2, however, occurs regioselectively at the 9-position. The reactivity behavior and regioselectivity of bromination of BN anthracenes are consistent with the electronic structure of these compounds; i.e., (1) the lower HOMO energy levels for BN anthracenes stabilize the molecules against cycloaddition and Friedel−Crafts reactions, and (2) the HOMO orbital coefficients are consistent with the observed bromination regioselectivity. Overall, this work demonstrates that BN/CC isosterism can be used as a molecular design strategy to stabilize the HOMO of acene-type structures while the optical band gap is maintained.

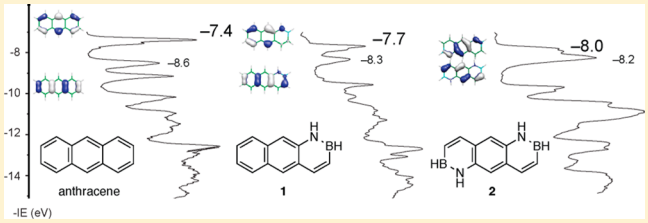

1. INTRODUCTION

Polycyclic aromatic hydrocarbons (PAHs) and their derivatives have received significant attention in materials research because of their modular synthetic access and their versatile, structure-dependent properties that make them useful as semiconductors in organic electronics applications.[1] BN/CC isosterism, i.e., the replacement of a C=C unit with the isosteric B−N unit, has emerged as a viable strategy to expand the chemical space of PAHs, leading to compounds with similar geometric parameters but quite distinct electronic structures.[2,3] Dewar pioneered the synthesis of BN isosteres of simple PAH in the 1950s and 1960s.[4] Among the compounds that Dewar and his co-workers prepared were 1,2-[5] and 9,10-BN naphthalenes,[6] 9,10-BN phenanthrenes,[7] 1,2-8,7-bis BN anthracenes,[8] 4a,10a-BN phenanthrene,[9] 4,5-9,10-bis BN pyrenes,[8] 5,6- and 6,5-BN benz[*a*]anthracenes,[10] 13,14-BN triphenylene,[11] 4,5-BN pyrene,[12] and 5,6-BN chrysene[12] (Scheme 1). Since Dewar's pioneering work, new methods for the preparation of existing and new BN isosteres of PAHs have been developed. With regard to bicyclic BN naphthalenes, Paetzold in 1968 prepared 1,2-BN naphthalenes via the condensation of arylchloro-(phenylamino)borane with phenylethyne.[13] In 2004, Paetzold adapted Dewar's original synthetic strategy to provide a comprehensive study of 1,2-BN naphthalenes, including ^{1}H, ^{13}C, and ^{11}B NMR characterization of two dozen derivatives, complexation studies with $(MeCN)_3Cr(CO)_3$, and establishing the equilibrium between the bis(azoniaboratanaphthyl) oxide and its corresponding monomeric BOH structure.[14] Ashe and co-workers used established synthetic methods to investigate the haptotropic migration of 1,2-BN naphthalenes,[15] and most recently, Molander's group established Suzuki−Miyaura and reductive cross-couplings of 3-bromo-1,2-BN naphthalenes.[16] The original synthesis of 9,10-BN naphthalene by Dewar via dehydrogenation of octahydro 9,10-BN naphthalene intermediate was low-yielding (~35%).[6a] Ashe and co-workers improved the synthetic access to 9,10-BN naphthalene by developing new synthetic methods based on the ring-closing metathesis (RCM)/dehydrogenation sequence.[17]

With regard to the tricyclic BN isosteres of PAHs, in addition to Dewar's extensive work from 1958 to 1961, Williams developed the oxidative photocyclization of anilinoboranes to prepare 9,10-BN phenanthrenes.[18] Additionally, Philp and co-workers investigated the hydrogen-bonding behavior of the

Received: August 26, 2014
Published: October 2, 2014

dx.doi.org/10.1021/ja508813v | J. Am. Chem. Soc. 2014, 136, 15414−15421

Scheme 1. Survey of Six-Membered-Ring-Containing BN Isosteres of PAHs Bearing Isolated BN Units

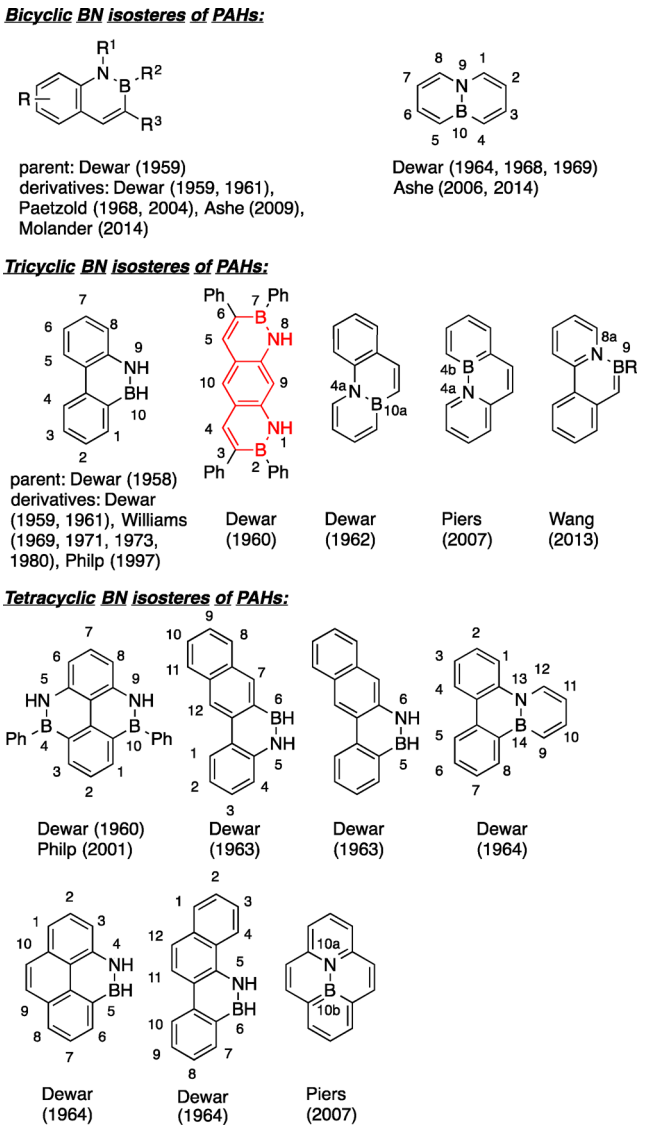

NH-BOH-9,10-BN phenanthrene system.[19] In 2007, Piers prepared the "internal" BN phenanthrene isostere 4a,4b-BN phenanthrene and found that its photophysical properties are distinct from the carbonaceous phenanthrene and Dewar's "external" 9,10-BN phenanthrene.[20] More recently, Wang prepared 8a,9-BN phenanthrene via the photoelimination of the corresponding cyclic pyridylborane precursor.[21] In addition to Dewar's initial work in the 1960s on tetracyclic BN isosteres of PAHs, Philp's group investigated the hydrogen-bonding behavior and dehydration reactivity of NH-BOH, 5,4-9,10-bis BN pyrene.[22] Furthermore, Piers and co-workers developed the synthesis of 10a,10b-BN pyrene, in which the BN unit is internalized.[23]

It was not until after 2010 when BN isosteres of PAHs have been demonstrated to have favorable charge transport properties. In 2011, Nakamura's group disclosed the synthesis of BN dibenzochrysene **A** and BN hexabenzotetracene **B** (Scheme 2) via an intramolecular electrophilic arene borylation and demonstrated that the intrinsic hole mobility of **A** (0.07 cm^2 V^{-1} s^{-1}) measured by time-resolved microwave conductivity is similar to that of rubrene and one order of magnitude better

Scheme 2. BN Heterocycles as Charge Transport Materials

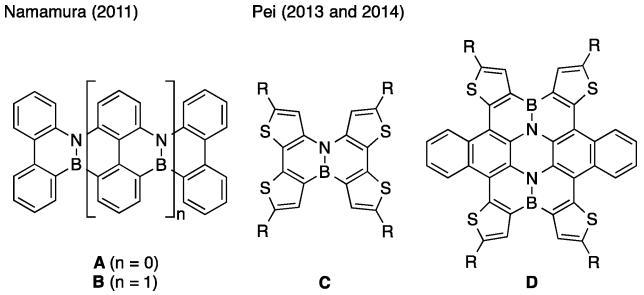

than the corresponding carbonaceous dibenzo[*g*,*p*]chrysene.[24] In 2013, Pei and co-workers synthesized BN-substituted tetrathienonaphthalenes **C** and reported a hole mobility of up to 0.15 cm^2 V^{-1} s^{-1} for organic field-effect transistor (OFET) devices based on those compounds.[25] Most recently in 2014, Pei and co-workers successfully synthesized BN coronene derivative **D** and fabricated OFET devices which exhibit a hole mobility of up to 0.23 cm^2 V^{-1} s^{-1}.[26]

Acenes, or linear benzofused polyaromatics, are a special class of PAH which possesses favorable properties for use in organic materials applications.[27] For instance, single-crystal organic field-effect transistors (SC-OFETs) based on rubrene (5,6,11,12-tetraphenyltetracene) have achieved a benchmark carrier mobility of 20–40 cm^2 V^{-1} s^{-1}.[28] Similarly, pentacene derivatives substituted at the 6- and 13-positions with alkynes have demonstrated a field-effect mobility of up to 0.4 cm^2 V^{-1} s^{-1} in organic thin-film transistors (OTFTs).[29] Furthermore, higher acenes, such as tetracene and pentacene derivatives, are uniquely capable of serving as singlet fission materials.[30]

Despite the useful properties of acenes and the important role they play in PAH chemistry, surprisingly few BN isosteres of higher acenes have been reported to date. Parental BN acene structures beyond the bicyclic naphthalene have remained elusive. To the best of our knowledge, the only example of a BN isostere of a higher acene is Dewar's 1,2-8,7-bis BN anthracene reported in 1960 (Scheme 1).[8] In this paper, we describe the synthesis of two parental BN-isosteres of anthracene (**1** and **2**) and their characterization, which includes ultraviolet photoelectron spectroscopy (UV-PES), optical properties, and chemical reactivity.

2. EXPERIMENTAL AND COMPUTATIONAL METHODS

Coupled UV-Photoelectron Spectroscopy–Mass Spectrometry Measurements. The UV-PES spectra were recorded on a home-built (IPREM/ECP), three-part spectrometer equipped with a main body device, He–I radiation source (21.21 and/or 48 eV), and a 127° cylindrical analyzer. The spectrometer works at constant analyzer energy under 5×10^{-6} hPa working pressure and $\leq 10^{-7}$ hPa for channeltron (X914L) pressure. The monitoring is done by a microcomputer supplemented by a digital-analogue converter (AEI spectrum). The spectra resulting from a single scan are built from 2048 points and are accurate within 0.05 eV. Spectra are calibrated with lines of xenon (12.13 and 13.44 eV) and of argon (15.76 and 15.94 eV). The accuracy of the ionization energies is ±0.03 eV for sharp peaks and ±0.05 eV for broad and overlapping signals. Mass spectra were recorded on a modified quadrupole mass spectrometer (PFEIFFER Prisma QMS200) with an electron impact at 50 eV (mass range, 200 amu; detection limit, $\leq 10^{-14}$ hPa; working pressure, 2×10^{-7} hPa; operating temperature, 200 °C; electronic amplifier in working conditions, 10^{-10} A; QUAD STAR422 software for recording and treatment of MS data). The samples were slowly vaporized under low pressure (10^{-6} hPa) inside a handmade three-valve injector ($^3/_4$ in.

dx.doi.org/10.1021/ja508813v | J. Am. Chem. Soc. 2014, 136, 15414–15421

diameter; 10 cm length; working temperature, −190 °C ≤ T ≤ 300 °C), and the gaseous flow was then continuously and simultaneously analyzed by both UV-photoelectron and mass spectrometers.

Computational Methods. All calculations were performed using the Gaussian 09[31] program package with the 6-311G(d,p)[32] basis set. Extra diffuse functions [6-311++G(d,p)] are included in the basis set to improve the description of the electron affinities (EAs). DFT has been shown to predict various molecular properties of similar compounds successfully.[33] All geometry optimizations were carried out with the CAM-B3LYP[34] functionals and were followed by frequency calculations in order to verify that the stationary points obtained were true energy minima. Ionization energies (IEs) were calculated with ΔSCF-DFT, which means that separate SCF calculations were performed to optimize the orbitals of the ground state and the appropriate ionic state (IE = $E_{cation} - E_{neutral}$). The advantages of the most frequently employed ΔSCF-DFT method of calculations of the first ionization energies have been demonstrated previously.[35] The TD-DFT[36,37] approach provides a first-principal method for the calculation of excitation energies within a density functional context taking into account the low-lying ion calculated by the ΔSCF method (the excitation energies of the radical cation obtained from a TD-DFT treatment were added to the ionization energy that was computed with the ΔSCF-DFT method). The vertical ionization energies were also calculated at the ab initio level according to the OVGF[38] (in this case the effects of electron correlation and reorganization are included beyond the Hartree−Fock approximation, and the self-energy part was expanded up to third order) and SAC−CI[39] (the symmetry adapted cluster/configuration interaction method of Nakatsuji and Hirao, which describes accurately and efficiently the electronic structures of the excited, ionized, and electron-attached states of molecules) methods. MOLEKEL[40] and GaussView were used as visualization tools for MOs.

3. RESULTS AND DISCUSSION

Synthesis. The syntheses of targeted compounds **1** and **2** were adapted from Dewar's original protocol for the preparation of 1,2-BN naphthalenes.[5] The key step involves the borylative cyclization of an aminostyrene. Commercially available starting material 3-amino-2-naphthoic acid **3** underwent a Sandmeyer reaction to generate the iodinated compound **4** in good yield (Scheme 3).[41] Subsequent Curtius

Scheme 3. Synthesis of 1,2-BN Anthracene 1

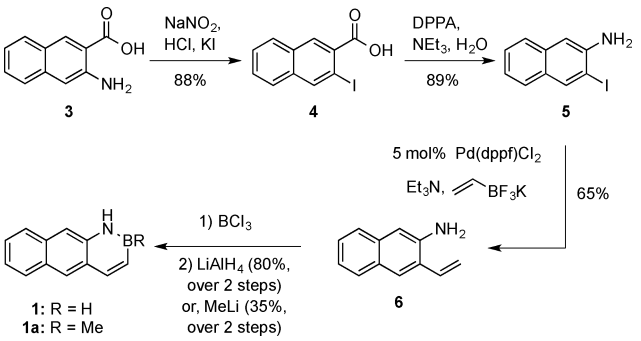

rearrangement of **4** using diphenylphosphoryl azide (DPPA) as the azide source resulted in the formation of 3-iodonaphthalen-2-amine **5**.[42] Suzuki cross-coupling of intermediate **5** with potassium vinyltrifluoroborate furnished 2-amino-3-vinylnaphthalene **6**.[43] Treatment of precursor **6** with boron trichloride followed by lithium aluminum hydride ($LiAlH_4$) produced 1,2-BN anthracene **1**. Alternatively, when MeLi is used as the nucleophile instead of $LiAlH_4$, the *B*-Me substituted 1,2-BN anthracene **1a** is generated. The parent 1,2-BN anthracene **1** is air-stable and can be readily purified by recrystallization from hot chlorobenzene. Starting with 10 g of **3**, we were able to synthesize up to 3.4 g of BN anthracene **1** in one batch without involvement of column chromatography and with an overall yield of 36%.[44]

The synthesis of bis-BN anthracene **2** commenced with the oxidation of commercially available 1,4-dibromo-2,5-dimethylbenzene **7** with $KMnO_4$[45] followed by Curtius rearrangement to produce N-Boc-protected dibromide **8** (Scheme 4). Cross-

Scheme 4. Synthesis of Bis-BN Anthracene 2

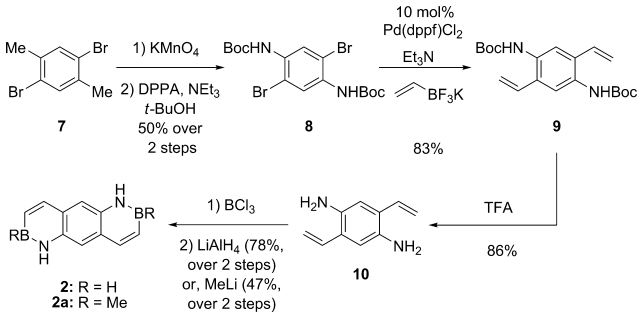

coupling of **8** with potassium vinyltrifluoroborate furnished the bis-vinyl adduct **9**. Removal of the *N*-Boc protecting group was accomplished with trifluoroacetic acid to reveal the key cyclization precursor **10**. Gratifyingly, double cyclization with boron trichloride proceeded smoothly, and subsequent treatment of the resulting crude mixture with $LiAlH_4$ gave bis-BN anthracene **2** in 78% yield over two steps. Alternatively, when the initial cyclized intermediate was treated with MeLi instead of $LiAlH_4$, bis-BN anthracene **2a** was produced.

UV-Photoelectron Spectroscopy. UV-PES experimentally determines the gas-phase ionization energies of molecules that can be correlated to the energies of occupied molecular orbitals. For a reliable assignment of UV photoelectron spectroscopic bands and for the interpretation of spectra, a combined UV-PES/theoretical approach is necessary. Chrostowska's group has calibrated different computational methods [e.g., the standard outer valence green function (OVGF), density functional theory (DFT), self-consistent field/time-dependent density functional theory (ΔSCF/TD-DFT), TD-DFT, complete active space second-order perturbation theory (CASPT2), and statistical average of different orbital model potential exchange−correlation functional (SAOP XC)] against the experimentally determined UV-PES IEs.[36] The combined UV-PES/computational modeling approach developed by Chrostowska and co-workers is used to investigate the electronic structure of BN anthracenes **1** and **2**.

Figure 1 illustrates the UV-PE spectra and the highest occupied MOs (HOMOs) corresponding to the experimentally determined IEs of each of the three anthracene molecules. The UV-PES of anthracene has been reported.[46] For the sake of consistency and to allow for a direct comparison among the compounds under investigation, we collected its UV-PES data again (Figure 1a). Its first ionization occurs at 7.4 eV and corresponds to ejection of an electron from the HOMO (b_{2g} symmetry). The second, third, and fourth ionizations occur at 8.6, 9.2, and 10.2 eV and correspond to HOMO−1 (b_{1g}), HOMO−2 (a_u), and HOMO−3 (b_{2g}), respectively. The first band of the PE spectrum of BN anthracene **1** (point group C_s) can be found at 7.7 eV and corresponds to its HOMO. This orbital has A″ symmetry and can be compared with the HOMO

dx.doi.org/10.1021/ja508813v | J. Am. Chem. Soc. 2014, 136, 15414−15421

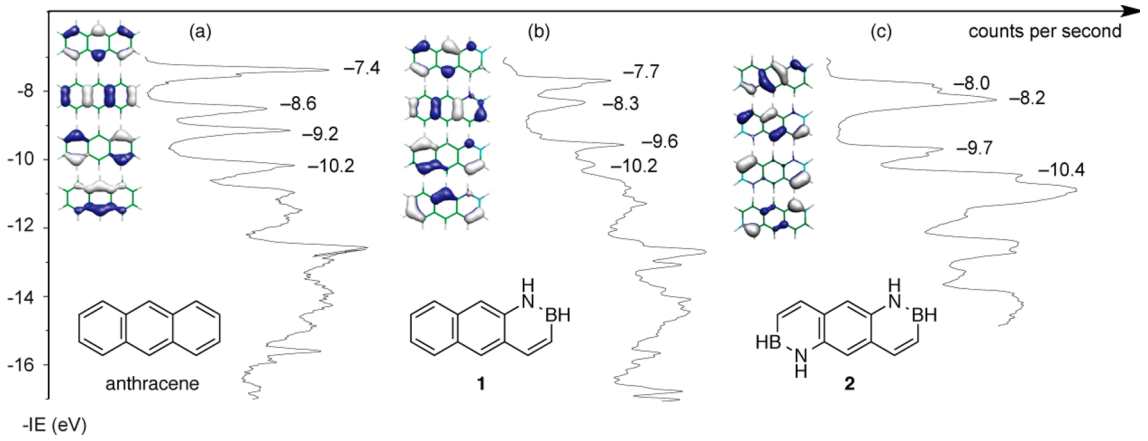

Figure 1. UV-PE spectra of (a) anthracene, (b) BN anthracene **1**, and (c) bis-BN anthracene **2**. The vertical axis is defined as the negative value of the experimentally determined ionization energy (−IE). The top four occupied molecular orbitals associated with the corresponding ionization energies for each of the molecules are also depicted.

of anthracene. The second (8.3 eV), third (9.6 eV), and fourth ionizations (10.2 eV) correspond to HOMO−1 (A″), HOMO−2 (A″), and HOMO−3 (A″), respectively. For bis-BN anthracene **2** (point group C_{2h}), the first ionization band was found at 8.0 eV (corresponding to the HOMO, b_g), followed by bands at 8.2 eV (b_g), 9.7 eV (a_u), and 10.4 eV (a_u). It is worth noting that the four highest occupied MOs for each anthracene molecule are π-type orbitals.

According the frontier molecular orbital theory,[47] the electronic structure determination of the HOMO and LUMO is most significant in terms of property and reactivity predictions. Figure 1 shows that for the anthracene system, a trend of decreasing HOMO energy levels with more BN units is observed: anthracene (−7.4 eV) > 1,2-BN anthracene **1** (−7.7 eV) > bis-BN anthracene (−8.0 eV). This is in stark contrast to simple monocyclic arenes, where BN/CC isosterism results in significant destabilization of the HOMO.[48,49] The stabilization of the HOMO is an important objective, as molecules with a high HOMO energy level typically lead to reactive, air sensitive materials.[50,51] Thus, our UV-PES analysis suggests that BN/CC isosterism could potentially serve as a design strategy to stabilize otherwise unstable PAHs compounds (e.g., higher acenes).

Absorption and Emission Spectra. Figure 2 illustrates the absorption spectra of anthracene, BN anthracene **1**, and bis-BN anthracene **2** in cyclohexane. The lowest-energy absorption peaks for BN anthracenes and the carbonaceous anthracene are all centered around 377 nm. This observation is again in contrast to the behavior of simple monocyclic arenes, for which it has been determined that BN/CC isosterism causes a significant bathochromic shift of the lowest-energy absorption band.[48,52] Figure 2 also shows that in contrast to the carbonaceous anthracene, a second electronic transition can be observed for BN anthracenes ($\lambda_{max(1)}$ = 327 nm, $\lambda_{max(2)}$ = 311 nm) in the 280−400 nm window. As is commonly seen with PAHs in nonpolar solutions, the vibrational fine structure for the electronic transitions illustrated in Figure 2 is well-resolved. According to TD-DFT calculations (see the Supporting Information for details), the lower-energy absorption band at ∼360 nm can be ascribed to the $S_0 \rightarrow S_1$ transition for all anthracene compounds.[53] This excitation mainly involves a HOMO → LUMO transition with relatively small oscillator strength. The high-energy band observed for BN anthracenes at

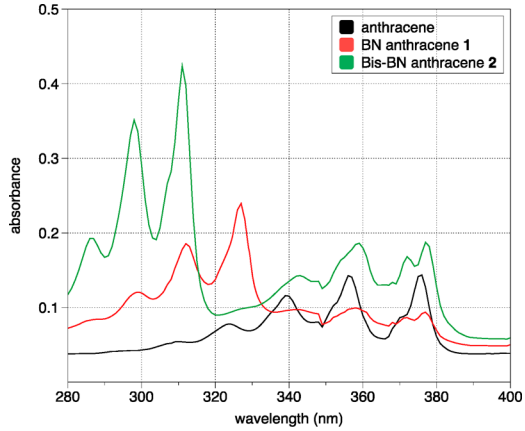

Figure 2. Absorption spectra of anthracene, BN anthracene **1**, and bis-BN anthracene **2** measured in cyclohexane at 5.5 × 10^{-6} M concentration.

∼310 nm is predicted to have a relatively strong oscillator strength and originates mostly from the transition of HOMO−1 → LUMO with some minor involvement of the LUMO+1 (for BN anthracene **1**) and LUMO+2 (for bis-BN anthracene **2**).

Figure 3 shows the emission spectra of anthracene, BN anthracene **1**, and bis-BN anthracene **2** in cyclohexane. The highest-energy emission peaks for the three anthracene molecules are located around 387 nm with vibrational energy levels being resolved. The difference between the lowest-energy *absorption* peak (377 nm) and the highest-energy *emission* peak (387 nm) is relatively small, suggesting a small structural reorganization going from the ground state to the first excited state.

The excitation spectra correlate with the absorption spectra for BN anthracenes **1** and **2**, and when the BN anthracenes are excited at either the low- or the high-energy absorption band in a nonpolar solvent, the resulting emission peaks are the same without loss of vibrational fine structure (see the Supporting Information for details). These observations are consistent with Kasha's rule; i.e., the observed emission bands originate from the lowest singlet excited state.[54]

The emission intensity at the highest-energy peak was linear from 4.5 × 10^{-6} to 1.8 × 10^{-5} M. At higher concentrations, the

dx.doi.org/10.1021/ja508813v | J. Am. Chem. Soc. 2014, 136, 15414−15421

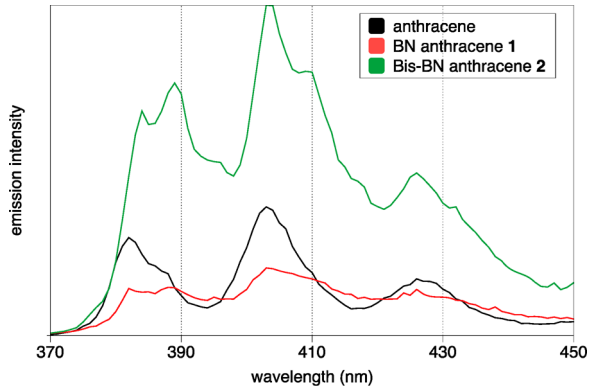

Figure 3. Emission spectra of anthracene, BN anthracene **1**, and bis-BN anthracene **2** measured in cyclohexane at 5.5 × 10^{-6} M concentration (excitation wavelength: 360 nm).

fluorescence did not increase linearly with concentration (see the Supporting Information for details), indicating concentration-dependent quenching. There was no evidence for excimer formation, as the emission profile remained unchanged over the range of concentrations that we investigated.[55,56] Compounds **1** and **2** have fluorescence quantum yields of 0.38 and 0.68, respectively; anthracene has a reported quantum yield of 0.36.[57]

The table and the orbital diagram in Figure 4 summarize key experimental data that describe the electronic structure of the anthracene series. From UV-PES studies we learned that the energy of the HOMO decreases in the order of anthracene > BN anthracene > bis-BN anthracene. According to the UV–vis absorption spectra, the estimated HOMO–LUMO gaps

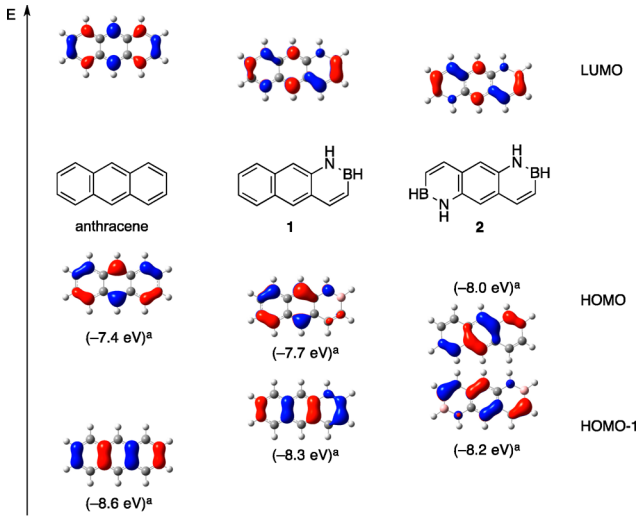

	E_{HOMO}[a]	E_{Gap}[b]	λ_{max1}	ε_1[c]	λ_{max2}	ε_2[d]	$\lambda_{max(em)}$[e]	Φ_F[f]
Anthracene	-7.4 eV	3.26 eV	-	-	356 nm	9700	403 nm	0.36
1	-7.7 eV	3.22 eV	327 nm	14000	359 nm	4900	403 nm	0.38
2	-8.0 eV	3.23 eV	311 nm	27000	357 nm	10000	403 nm	0.68

[a] Determined by UV-PES. [b] Determined by UV-Vis spectroscopy in cyclohexane solution (the intersection of the "wavelength" axis and the tangent passing through the inflection point of the lowest-energy absorption peak). [c] Molar absorptivity constant at high-energy band (327 nm for **1** and 311 nm for **2**) in (L mol^{-1} cm^{-1}). [d] Molar absorptivity constant at low-energy band, 356 nm for anthracene, 359 nm for **1**, and 357 nm for **2**) in (L mol^{-1} cm^{-1}). [e]Wavelength of highest emission intensity. [f] Determined by the comparative method using anthracene (Φ_F = 0.36) and phenylanthracene (Φ_F = 0.49) in cyclohexane as the standards.

Figure 4. Summary of key experimental data.

(corresponding to the low-energy peak)[58] remain similar for all three anthracenes: anthracene, 3.26 eV; BN anthracene **1**, 3.22 eV; and bis-BN anthracene, 3.23 eV. TD-DFT calculations show that the $S_0 \rightarrow S_2$ transition mostly originates from the excitation of electrons in the HOMO−1 orbital, and UV-PES data show a destabilizing trend of the HOMO−1 energy with increasing BN units. Thus, the observation of an additional absorption band within the 280–400 nm window for the BN anthracenes **1** and **2** is consistent with their high-lying HOMO−1 and low-lying LUMO orbitals relative to those of anthracene (Figure 4).[59]

Survey of Reactivity. We have determined that both BN anthracenes **1** and **2** exhibit good air stability, much like Dewar's 1,2-BN naphthalene.[5a] Samples of each **1** and **2** do not show appreciable decomposition by ^{1}H NMR analysis when left open to air and light on the benchtop for 7 days. We attempted to determine the pK_a of **1** using a bracketing study. However, when we treated **1** with potassium hexamethyldisilazide (KHMDS) to deprotonate the *N*-H proton, we observed addition to boron. To avoid complications associated with the reactivity of the *B*–H group, we performed all further reactivity studies on the *B*–Me derivatives **1a** and **2a.**

KHMDS cleanly deprotonates **1a** at nitrogen to furnish the corresponding conjugate base of **1a**. By quenching this anion with a variety of potential proton sources, we determined that the pK_a of **1a** is approximately 26; the anion partially deprotonated pentamethylcyclopentadiene (Cp*H) (pK_a = 26 in DMSO), as evidenced by peaks for both $C_5Me_5^-$ and C_5Me_5H in the ^{1}H NMR spectrum. Ashe and co-workers similarly observed partial deprotonation of Cp*H when they treated it with the anion of monocyclic *B*-phenyl-1,2-azaborine and assigned its pK_a at approximately 26.[60] Using the same method, the pK_a of bis-BN anthracene **2a** was determined to be also ∼26.

The cycloaddition chemistry of anthracene is well-known.[61] Both catalyzed and uncatalyzed Diels–Alder reactions occur across the central ring (Scheme 5).[62] We replicated these

Scheme 5. Survey of Cycloaddition and Friedel–Crafts-Type Reactivity

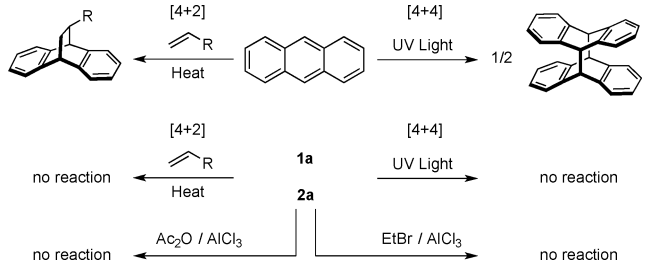

reaction conditions to attempt a [4 + 2] cycloaddition. When we treated **1a** or **2a** with a variety of dienophiles, we did not observe cycloaddition reactions (see the Supporting Information for details). The very electron deficient tetracyanoethylene dienophile, for example, did not react with **1a** or **2a** when heated up to 130 °C in benzene-d_6. Under identical conditions, anthracene fully converted to the cycloaddition product within hours.[63] Iron(III)- and aluminum(III)-catalyzed conditions[64] also did not produce any cycloadducts. We also attempted to use compound **1a** as a dienophile instead of a diene, and no reaction was observed.

dx.doi.org/10.1021/ja508813v | J. Am. Chem. Soc. 2014, 136, 15414–15421

It is known that UV light induces a [4 + 4] dimerization across anthracene's central ring, yielding the so-called "butterfly" dimer (Scheme 5).[61] We did not observe a [4 + 4] dimerization reaction when we irradiated **1a** or **2a** with UV light. Similarly, neither compound **1a** nor **2a** undergoes a Friedel–Crafts alkylation when treated with ethyl bromide in the presence of a Lewis acid (e.g., iron trichloride or aluminum trichloride). We were able to recover only starting materials with no evidence of reaction, even with excess Lewis acid present. Attempted Friedel–Crafts acylation[65] reactions of **1a** or **2a** using acetic anhydride and aluminum trichloride were similarly ineffective. The generally observed lack of cycloaddition and Friedel–Crafts reactivity for BN anthracenes is consistent with their relatively low-lying HOMO energy levels as determined by UV-PES.

Despite the relatively low propensity of BN anthracenes to undergo cycloaddition and Friedel–Crafts reactions, they do react with halogens.[66] For instance, treatment of **1a** with elemental bromine at 0 °C generates the brominated BN anthracene **1a-Br** regioselectively in good yield (Figure 5).[67]

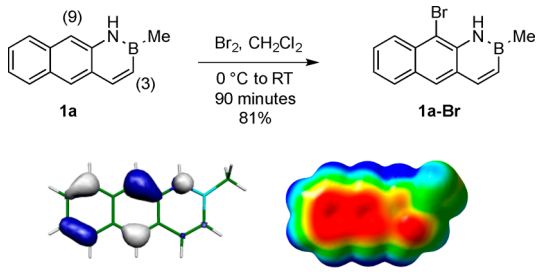

Figure 5. Regioselective halogenation of BN anthracenes **1**.

The electrophilic halogenations of **1a** preferentially take place at the 9-position, which is in stark contrast to what has been observed for 1,2-BN naphthalenes,[5b,16a] 9,10-BN naphthalenes,[6b] and monocyclic 1,2-azaborines,[68] where the carbon adjacent to boron has been determined to be the most reactive position. As can be seen from Figure 5, the HOMO orbital coefficient at the 9-position for **1a** is relatively large while the corresponding coefficients at the C(3) position are diminishingly small (Figure 5, bottom left). On the other hand, while the electrostatic potential map for **1a** indicates a significant negative charge at the 9-position, substantial negative charge is also located at the C(3) position (Figure 5, bottom right). Thus, it appears that the reaction of BN anthracenes **1a** with Br_2 is orbitally controlled, which is consistent with the "soft" nature of the electrophilic Br_2 reagent.[47b,69]

To further support our assignment of the regioselective bromination reaction, we prepared BN anthracene **1b-TPA** from BN anthracene **1b** by using the previously employed bromination conditions followed by Suzuki cross-coupling with (4-(diphenylamino)phenyl)boronic acid (Scheme 6). Crystals of **1b-TPA** suitable for single-crystal X-ray diffraction analysis were grown from a pentane/Et_2O solution of **1b-TPA**, and the structure illustrated in Scheme 6 unambiguously confirms our regiochemical assignment of the bromination reaction.[70]

4. CONCLUSION

In summary, we prepared the first parental BN anthracenes **1** and **2** and characterized their electronic structure and reactivity behavior in direct comparison with the carbonaceous anthracene. Gas-phase UV-PES studies revealed the following

Scheme 6. Synthesis and Crystallographic Characterization of 1b-TPA

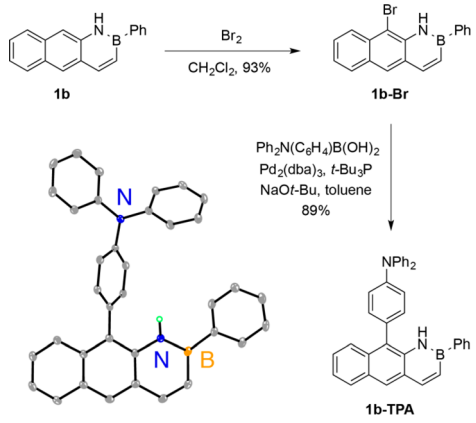

HOMO energy trend: anthracene, −7.4 eV; BN anthracene **1**, −7.7 eV; bis-BN anthracene **2**, −8.0 eV. In stark contrast to monocyclic arenes, BN/CC isosterism in the context of anthracene leads to stabilization of the HOMO. The absorption behaviors of the low-energy band of the anthracene series (i.e., anthracene, **1**, and **2**) are similar, which is also in contrast to the monocyclic system, where a bathochromic shift was observed for BN isosteres of benzene and toluene vs their carbonaceous counterparts. The λ_{max} of the lower energy band in the UV–vis absorption spectrum is as follows: anthracene, 356 nm; BN anthracene **1**, 359 nm; bis-BN anthracene **2**, 357 nm. The HOMO–LUMO band gap remains unchanged across the anthracene series. Consistent with Kasha's rule, the emission for the anthracene series originates from the corresponding singlet excited states. The emission λ_{max} for the three investigated anthracene compounds are all at 403 nm. We determined the pK_a of the *N*-H proton for BN anthracene **1** and bis-BN anthracene **2** to be approximately 26. In contrast to anthracene, its BN isosteres **1** and **2** do not undergo thermal or photoinduced cycloaddition reactions and Friedel–Crafts acylations. BN anthracene **1a**, however, undergoes regioselective electrophilic bromination with Br_2 at the 9-position. The reactivity behavior of BN anthracenes is consistent with the electronic structure of these compounds; i.e., (1) the lower HOMO energy levels for BN anthracenes stabilize the molecules against cycloaddition and Friedel–Crafts reactions, and (2) the HOMO orbital coefficients are consistent with the observed bromination regioselectivity. Overall, this work demonstrates that BN/CC isosterism can be used as a molecular design strategy to stabilize the HOMO of acene-type structures while the optical band gap is maintained. Current efforts are directed at developing BN isosteres of higher linear acenes.

■ ASSOCIATED CONTENT

Supporting Information

Experimental procedures, spectroscopic data, additional computational details, complete ref 31, and crystallographic information, including CIF files. This material is available free of charge via the Internet at http://pubs.acs.org.

■ AUTHOR INFORMATION

Corresponding Authors

shihyuan.liu@bc.edu;
anna.chrostowska@univ.pau.fr

Author Contributions

[⊥]J.S.A.I. and J.L.M. contributed equally to this paper.

Notes

The authors declare no competing financial interest.

■ ACKNOWLEDGMENTS

This paper is dedicated to Prof. Lawrence T. Scott on the occasion of his 70th birthday. Support has been provided by the Defense Threat Reduction Agency (Grant HDTRA1-11-1-0045). We thank Prof. Michael M. Haley for helpful discussions. A.C. and A.M. are grateful to the Communauté de Communes de Lacq (France) for financial support.

■ REFERENCES

(1) For an overview, see the following: (a) Wang, C.; Dong, H.; Hu, W.; Liu, Y.; Zhu, D. *Chem. Rev.* **2012**, *112*, 2208−2267. (b) Wu, J.; Pisula, W.; Müllen, K. *Chem. Rev.* **2007**, *107*, 718−747. (c) Watson, M. D.; Fechtenkötter, A.; Müllen, K. *Chem. Rev.* **2001**, *101*, 1267−1300. (d) Mitschke, U.; Bauerle, P. *J. Mater. Chem.* **2000**, *10*, 1471−1507. Yamashita, Y. *Sci. Technol. Adv. Mater.* **2009**, *10*, 024313.

(2) For an overview, see the following: (a) Bosdet, M. J. D.; Piers, W. E. *Can. J. Chem.* **2009**, *87*, 8−29. (b) Campbell, P. G.; Marwitz, A. J.; Liu, S.-Y. *Angew. Chem., Int. Ed.* **2012**, *51*, 6074−6092. (c) Liu, Z.; Marder, T. B. *Angew. Chem., Int. Ed.* **2008**, *47*, 242−244.

(3) For recent examples, see the following: (a) Braunschweig, H.; Damme, A.; Jimenez-Halla, J. O.; Pfaffinger, B.; Radacki, K.; Wolf, J. *Angew. Chem., Int. Ed.* **2012**, *51*, 10034−10037. (b) Brown, A. N.; Zakharov, L. N.; Mikulas, T.; Dixon, D. A.; Liu, S.-Y. *Org. Lett.* **2014**, *16*, 3340−3343. (c) Xu, S.; Haeffner, F.; Li, B.; Zakharov, L. N.; Liu, S.-Y. *Angew. Chem., Int. Ed.* **2014**, *53*, 6795−6799. (d) Abbey, E. R.; Lamm, A. N.; Baggett, A. W.; Zakharov, L. N.; Liu, S.-Y. *J. Am. Chem. Soc.* **2013**, *135*, 12908−12913. (e) Xu, S.; Mikulas, T. C.; Zakharov, L. N.; Dixon, D. A.; Liu, S.-Y. *Angew. Chem., Int. Ed.* **2013**, *52*, 7527−7531. (f) Xu, S.; Zakharov, L. N.; Liu, S.-Y. *J. Am. Chem. Soc.* **2011**, *133*, 20152−20155. (g) Abbey, E. R.; Zakharov, L. N.; Liu, S.-Y. *J. Am. Chem. Soc.* **2011**, *133*, 11508−11511. (h) Daly, A. M.; Tanjaroon, C.; Marwitz, A. J.; Liu, S.-Y.; Kukolich, S. G. *J. Am. Chem. Soc.* **2010**, *132*, 5501−5506. (i) Marwitz, A. J.; McClintock, S. P.; Zakharov, L. N.; Liu, S.-Y. *Chem. Commun.* **2010**, *46*, 779−781.

(4) For an overview of Dewar's work, see the following: Fritsch, A. J. *Chem. Heterocycl. Compd.* **1977**, *30*, 381−440.

(5) (a) Dewar, M. J. S.; Dietz, R. *J. Chem. Soc.* **1959**, 2728−2730. (b) Dewar, M. J. S.; Dietz, R. *J. Org. Chem.* **1961**, *26*, 3253−3256.

(6) (a) Dewar, M. J. S.; Gleicher, G. J.; Robinson, B. P. *J. Am. Chem. Soc.* **1964**, *86*, 5698−5699. (b) Dewar, M.; Jones, R. *J. Am. Chem. Soc.* **1968**, *90*, 2137−2144. (c) Davis, F. A.; Dewar, M. J. S.; Jones, R.; Worley, S. D. *J. Am. Chem. Soc.* **1969**, *91*, 2094−2097.

(7) (a) Dewar, M. J. S.; Kubba, V. P.; Pettit, R. *J. Chem. Soc.* **1958**, 3073−3076. (b) Dewar, M. J. S.; Kubba, V. P. *Tetrahedron* **1959**, *7*, 213−222. (c) Dewar, M. J. S.; Dietz, R.; Kubba, V. P.; Lepley, A. R. *J. Am. Chem. Soc.* **1961**, *83*, 1754−1756. (d) Dewar, M. J. S.; Maitlis, P. M. *J. Am. Chem. Soc.* **1961**, *83*, 187−193. (e) Dewar, M. J. S.; Kubba, V. P. *J. Am. Chem. Soc.* **1961**, *83*, 1757−1760.

(8) Chissick, S. S.; Dewar, M. J. S.; Maitlis, P. M. *Tetrahedron. Lett.* **1960**, *1*, 8−10.

(9) Dewar, M. J. S.; Kaneko, C.; Bhattacharjee, M. K. *J. Am. Chem. Soc.* **1962**, *84*, 4884−4887.

(10) Dewar, M. J. S.; Poesche, W. H. *J. Am. Chem. Soc.* **1963**, *85*, 2253−2256.

(11) Culling, G. C.; Dewar, M. J. S.; Marr, P. A. *J. Am. Chem. Soc.* **1964**, *86*, 1125−1127.

(12) Dewar, M. J. S.; Poesche, W. H. *J. Org. Chem.* **1964**, *29*, 1757−1762.

(13) Paetzold, P. I.; Stohr, G.; Maisch, H.; Lenz, H. *Chem. Ber.* **1968**, *101*, 2881−2888.

(14) Paetzold, P.; Stanescu, C.; Stubenrauch, J. R.; Bienmuller, M.; Englert, U. *Z. Anorg. Allg. Chem.* **2004**, *630*, 2632−2640.

(15) Pan, J.; Kampf, J. W.; Ashe, A. J., III *Organometallics* **2009**, *28*, 506−511.

(16) (a) Molander, G. A.; Wisniewski, S. R. *J. Org. Chem.* **2014**, *79*, 6663−6678. (b) Molander, G. A.; Wisniewski, S. R.; Traister, K. M. *Org. Lett.* **2014**, *16*, 3692−3695.

(17) (a) Fang, X.; Yang, H.; Kampf, J. W.; Holl, M. M. B.; Ashe, A. J., III *Organometallics* **2006**, *25*, 513−518. (b) Rohr, A. D.; Kampf, J. W.; Ashe, A. J., III *Organometallics* **2014**, *33*, 1318−1321.

(18) (a) Grisdale, P. J.; Williams, J. L. R. *J. Org. Chem.* **1969**, *34*, 1675−1677. (b) Grisdale, P.; Glogowski, M.; Williams, J. L. R. *J. Org. Chem.* **1971**, *36*, 3821−3824. (c) Glogowski, M. E.; Grisdale, P. J.; Williams, J. L. R.; Regan, T. H. *J. Organomet. Chem.* **1973**, *54*, 51−60. (d) Glogowski, M. E.; Williams, J. L. R. *J. Organomet. Chem.* **1980**, *195*, 123−135.

(19) (a) Harris, K. D. M.; Kariuki, B. M.; Lambropoulos, C.; Philp, D.; Robinson, J. M. *Tetrahedron* **1997**, *53*, 8599−8612. (b) Robinson, J.; Kariuki, B. M.; Philp, D.; Harris, K. D. M. *Tetrahedron Lett.* **1997**, *38*, 6281−6284.

(20) Bosdet, M. J.; Jaska, C. A.; Piers, W. E.; Sorensen, T. S.; Parvez, M. *Org. Lett.* **2007**, *9*, 1395−1398.

(21) Lu, J. S.; Ko, S. B.; Walters, N. R.; Kang, Y.; Sauriol, F.; Wang, S. *Angew. Chem., Int. Ed.* **2013**, *52*, 4544−4548.

(22) Ashton, P. R.; Harris, K. D. M.; Kariuki, B. M.; Philp, D.; Robinson, J. M. A.; Spencer, N. *J. Chem. Soc., Perkin. Trans. 2* **2001**, 2166−2173.

(23) Bosdet, M. J.; Piers, W. E.; Sorensen, T. S.; Parvez, M. *Angew. Chem., Int. Ed.* **2007**, *46*, 4940−4943.

(24) Hatakeyama, T.; Hashimoto, S.; Seki, S.; Nakamura, M. *J. Am. Chem. Soc.* **2011**, *133*, 18614−18617.

(25) Wang, X. Y.; Lin, H. R.; Lei, T.; Yang, D. C.; Zhuang, F. D.; Wang, J. Y.; Yuan, S. C.; Pei, J. *Angew. Chem., Int. Ed.* **2013**, *52*, 3117−3120.

(26) Wang, X. Y.; Zhuang, F. D.; Wang, R. B.; Wang, X. C.; Cao, X. Y.; Wang, J. Y.; Pei, J. *J. Am. Chem. Soc.* **2014**, *136*, 3764−3767.

(27) For an overview, see the following: (a) Anthony, J. E. *Chem. Rev.* **2006**, *106*, 5028−5048. (b) Anthony, J. E. *Angew. Chem., Int. Ed.* **2008**, *47*, 452−483.

(28) Hasegawa, T.; Takeya, J. *Sci. Technol. Adv. Mater.* **2009**, *10*, 024314.

(29) Sheraw, D.; Jackson, N.; Eaton, L.; Anthony, E. *Adv. Mater.* **2003**, *15*, 2009−2011.

(30) (a) Congreve, D. N.; Lee, J.; Thompson, N. J.; Hontz, E.; Yost, S. R.; Reusswig, P. D.; Bahlke, M. E.; Reineke, S.; Van Voorhis, T.; Baldo, M. A. *Science* **2013**, *340*, 334−337. (b) Burdett, J. J.; Bardeen, C. J. *J. Am. Chem. Soc.* **2012**, *134*, 8597−8607. (c) Chan, W. L.; Ligges, M.; Zhu, X. Y. *Nat. Chem.* **2012**, *4*, 840−845.

(31) Frisch, M. J.; et al. *Gaussian 09*, revision B.01; Gaussian, Inc.: Wallingford, CT, 2009.

(32) Raghavachari, K.; Binkley, J. S.; Seeger, R.; Pople, J. A. J. *Chem. Phys.* **1980**, *72*, 650−654.

(33) (a) Parr, R. G.; Yang, W. *Functional Theory of Atoms and Molecules*; Oxford University Press: New York, 1989. (b) Frisch, M. J.; Trucks,G. W.;Cheeseman, J. R. In *Recent Development and Applications of Modern Density Functional Theory, Theoretical and Computational Chemistry*; Semminario, J. M., Ed.; Elsevier: Amsterdam, 1996; Vol. *4*; pp 679−707. (c) Limacher, P. A.; Mikkelsen, K. V.; Luthi, H. P. *J. Chem. Phys.* **2009**, *130*, 194114. (d) Kobayashi, R.; Amos, R. D. *Chem. Phys. Lett.* **2006**, *420*, 106−109. (e) Jacquemin, D.; Perpète, E. A.; Scalmani, G.; Frisch, M. J.; Kobayashi, R.; Adamo, C. *J. Chem. Phys.* **2007**, *126*, 144105.

(34) (a) Becke, A. D. *Phys. Rev.* **1988**, *38*, 3098−3100. (b) Becke, A. D. *J. Chem. Phys.* **1993**, *98*, 5648−5652. (c) Lee, C.; Yang, W.; Parr, R. G. *Phys. Rev. B* **1988**, *37*, 785−789. (d) Yanai, T.; Tew, D.; Handy, N. *Chem. Phys. Lett.* **2004**, *393*, 51−57.

(35) (a) Bartnik, R.; Bayleŕe, P.; Chrostowska, A.; Galindo, A.; Lesniak, S.; Pfister-Guillouzo, G. *Eur. J. Org. Chem.* **2003**, 2475−2479.. (b) Chrostowska, A.; Matrane, A.; Maki, D.; Khayar, S.; Ushiki, H.; Graciaa, A.; Belachemi, L.; Guillemin, J.-C. *ChemPhysChem* **2012**, *13*, 226−236.. (c) Chrostowska, A.; Dargelos, A.; Khayar, S.; Wentrup, C.

J. Phys. Chem. A **2012**, *116*, 9315−9320. (d) Vu, T. Y.; Chrostowska, A.; Huynh, T. K. X; Khayar, S.; Dargelos, A.; Justyna, K.; Pasternak, B.; Lesniak, S.; Wentrup, C. *Chem.—Eur. J.* **2013**, *19*, 14983−14988.
(36) Lemierre, V.; Chrostowska, A.; Dargelos, A.; Chermette, H. *J. Phys. Chem. A* **2005**, *109*, 8348−8355.
(37) (a) Stratmann, R. E.; Scuseria, G. E.; Frisch, M. J. *J. Chem. Phys.* **1998**, *109*, 8218−8224. (b) Casida, M. E.; Jamorski, C.; Casida, K. C.; Salahub, D. R. *J. Chem. Phys.* **1998**, *108*, 4439−4449.
(38) (a) von Niessen, W.; Schirmer, J.; Cederbaum, L. S. *Comput. Phys. Rep* **1984**, *1*, 57−125. (b) Ortiz, J. V. *J. Chem. Phys.* **1988**, *89*, 6348−6352.
(39) Nakatsuji, H.; Hirao, K. *J. Chem. Phys.* **1978**, *68*, 2053−2065. See also the following: http://www.qcri.or.jp/sacci/ (accessed August 2014).
(40) (a) Portmann, S.; Luthi, H. P. *MOLEKEL 4.3*; Swiss National Supercomputing Center: Lugano, Switzland. (b) Portmann, S.; Luthi, H. P. *CHIMIA* **2000**, *54*, 766−770.
(41) Uyanik, M.; Akakura, M.; Ishihara, K. *J. Am. Chem. Soc.* **2009**, *131*, 251−262.
(42) Shioiri, T.; Ninomiya, K.; Yamada, S. *J. Am. Chem. Soc.* **1972**, *94*, 6203−6205.
(43) Molander, G. A.; Bernardi, C. R. *J. Org. Chem.* **2002**, *67*, 8424−8429.
(44) The yields reported in Scheme 3 are the optimized yields for each of the individual steps.
(45) Surampudi, S. K.; Nagarjuna, G.; Okamoto, D.; Chaudhuri, P. D.; Venkataraman, D. *J. Org. Chem.* **2012**, *77*, 2074−2079.
(46) Rademacher, P.; Kettler, B.; Kowski, K.; Weiss, M. E. *Spectrochim. Acta, Part A* **2001**, *57*, 2475−2483.
(47) (a) Fukui, K.; Yonezawa, T.; Shingu, H. *J. Chem. Phys.* **1952**, *20*, 722−725. (b) Fleming, I. *Frontier Orbitals and Organic Chemical Reactions*; Wiley: London, 1978.
(48) Chrostowska, A.; Xu, S.; Lamm, A. N.; Mazière, A.; Weber, C. D.; Dargelos, A.; Baylère, P.; Graciaa, A.; Liu, S.-Y. *J. Am. Chem. Soc.* **2012**, *134*, 10279−10285.
(49) The HOMO energy levels of the indole system appear to be unperturbed by BN/CC isosterism; see the following: Chrostowska, A.; Xu, S.; Mazière, A.; Boknevitz, K.; Li, B.; Abbey, E. R.; Dargelos, A.; Graciaa, A.; Liu, S.-Y. *J. Am. Chem. Soc.* **2014**, *136*, 11813−11820.
(50) Takimiya, K.; Yamamoto, T.; Ebata, H.; Izawa, T. *Sci. Technol. Adv. Mater.* **2007**, *8*, 273−276.
(51) The HOMO−LUMO gap has also been demonstrated to influence the kinetic stability of polycyclic aromatic hydrocarbons; see the following: (a) Aihara, J.-I. *J. Phys. Chem. A* **1999**, *103*, 7487−7495. (b) Kaur, I.; Jia, W.; Kopreski, R. P.; Selvarasah, S.; Dokmeci, M. R.; Pramanik, C.; McGruer, N. E.; Miller, G. P. *J. Am. Chem. Soc.* **2008**, *130*, 16274−16286.
(52) (a) Marwitz, A. J. V.; Matus, M. H.; Zakharov, L. N.; Dixon, D. A.; Liu, S.-Y. *Angew. Chem., Int. Ed.* **2009**, *48*, 973−977. (b) Marwitz, A. J. V.; Lamm, A. N.; Zakharov, L. N.; Vasiliu, M.; Dixon, D. A.; Liu, S.-Y. *Chem. Sci.* **2012**, *3*, 825−829. (c) Taniguchi, T.; Yamaguchi, S. *Organometallics* **2010**, *29*, 5732−5735.
(53) For an overview on the photophysical characterization and photochemistry of anthracene, see the following: Becker, H.-D. *Chem. Rev.* **1993**, *93*, 145−172.
(54) Kasha, M. *Discuss. Faraday. Soc.*. **1950**, *9*, 14−19.
(55) Saigusa, H.; Lim, E. C. *Acc. Chem. Res.* **1996**, *29*, 171−178.
(56) The low solubility of these compounds limited our investigation of emission as a function of concentration.
(57) Berlman, I. B. *Handbook of Fluorescence Spectra of Aromatic Molecules*; Academic Press: New York, 1971.
(58) The HOMO−LUMO optical band gap has been estimated using the intersection of the *x*-axis by the line tangent to the onset of the lowest-energy absorption peak. For examples see the following: (a) Chase, D. T.; Rose, B. D.; McClintock, S. P.; Zakharov, L. N.; Haley, M. M. *Angew. Chem., Int. Ed.* **2011**, *50*, 1127−1130. (b) Popere, B. C.; Della Pelle, A. M.; Poe, A.; Balaji, G.; Thayumanavan, S. *Chem. Sci.* **2012**, *3*, 3093−3102.
(59) According to Figure 2, the $S_0 \rightarrow S_2$ transition is higher in energy for bis-BN anthracene **2** than for BN anthracene **1**. This may be due to the predicted involvement of the high-energy HOMO-1 → LUMO+2 transition for **2**, which is not predicted for compound **1**.
(60) Pan, J.; Kampf, J. W.; Ashe, A. J., III *Organometallics* **2004**, *23*, 5626−5629.
(61) For a review, see the following: Atherton, J. C. C.; Jones, S. *Tetrahedron* **2003**, *59*, 9039−9057.
(62) For an example, see the following: Fort, E. H.; Scott, L. T. *Angew. Chem., Int. Ed.* **2010**, *49*, 6626−6628.
(63) Lotfi, M.; Roberts, R. M. G. *Tetrahedron* **1979**, *35*, 2131−2136.
(64) Yates, P.; Eaton, P. *J. Am. Chem. Soc.* **1960**, *82*, 4436−4437.
(65) Ball, J. C.; Brennan, P.; Elsunaki, T. M.; Jaunet, A.; Jones, S. *Tetrahedron: Asymmetry* **2011**, *22*, 253−255.
(66) Heilbron, I. M.; Heaton, J. S. *Org. Synth.* **1923**, *3*, 41.
(67) Treatment of **1a** with **2** equiv of bromine produced a relatively complex mixture of products. BN-anthracene **2a** gave a mixture of compounds under identical electrophilic bromination conditions as illustrated in Figure 5 in low yield.
(68) (a) Pan, J.; Kampf, J. W.; Ashe, A. J., III *Org. Lett.* **2007**, *9*, 679−681. (b) Lamm, A. N.; Liu, S.-Y. *Mol. BioSyst.* **2009**, *5*, 1303−1305.
(69) (a) Pearson, R. G. *J. Chem. Educ.* **1968**, *45*, 581−587. (b) Pearson, R. G. *J. Chem. Educ.* **1968**, *45*, 643−648. (c) Ho, T.-L. *Chem. Rev.* **1975**, *75*, 1−20.
(70) The crystal structure for **1b** shows a herringbone-type, edge-to-face packing motif (see the Supporting Information for details). Multiple attempts at crystallization of **1**, **2**, **1a**, **1a-Br**, and **2a** yielded crystals unsuitable for single-crystal X-ray diffraction.